In Silico Research in Biomedicine xxx (xxxx) 100054

Contents lists available at ScienceDirect

In Silico Research in Biomedicine

journal homepage: www.elsevier.com

Solid lipid nanoparticle encapsulated beta-carotene for targeted breast cancer therapy: Network pharmacology, molecular docking, and in vitro evaluation

Kandanagolla Sumalatha *, Panneerselvam Theivendren *, Gandhimathi Rathinasamy *

Department of Pharmaceutical Chemistry & Analysis, School of Pharmaceutical Sciences, Vels Institute of Science, Technology & Advanced Studies, Pallavaram, Chennai, Tamilnadu 600117, India

ARTICLE INFO

Keywords:
Breast cancer
Beta-carotene
Natural drugs
Immunotherapy
Antioxidants
Apoptosis
Molecular Modelling

ABSTRACT

The present study investigates the potential of beta-carotene–encapsulated solid lipid nanoparticles (SLNs) as a targeted therapeutic approach for breast cancer treatment. Utilizing a combination of network pharmacology, molecular docking, and molecular dynamics simulations, the interactions between beta-carotene and key oncogenic proteins were systematically analyzed. Findings revealed that beta-carotene exhibited a strong inhibitory effect on cancer cell proliferation, primarily by inducing apoptosis and suppressing metastatic progression. Pharmacokinetic profiling through ADMET (Absorption, Distribution, Metabolism, Excretion, and Toxicity) analysis confirmed favorable drug-like properties of beta-carotene, supporting its suitability as a therapeutic candidate. The formulated SLNs demonstrated an encapsulation efficiency of 84 ± 1.12 % and a drug loading capacity of 8.47 ± 0.93 %, indicating effective incorporation of beta-carotene into the lipid matrix. In vitro release studies revealed a controlled release pattern following a first-order kinetic model, with 40.21 % drug release at pH 5.2 and 27.11 % at pH 7.5 within 5 h, suggesting pH-dependent release behavior beneficial for tumor microenvironment targeting. The cytotoxic evaluation using the MCF-7 breast cancer cell line yielded an IC_{50} value of 22.82 μg/mL, signifying moderate cytotoxic activity. These results underscore the promise of beta-carotene-loaded SLNs as a novel, bioavailable nanocarrier system for breast cancer therapy. The encapsulation process not only enhances the stability of beta-carotene but also significantly improves its bioavailability, making it a compelling candidate for further clinical translation. To fully realize its therapeutic potential, additional studies focusing on long-term formulation stability, optimized release kinetics, and in vivo therapeutic efficacy are recommended. Such investigations will pave the way for developing more effective and natural treatment strategies against breast cancer, harnessing the synergistic benefits of nanotechnology and bioactive natural compounds.

Introduction

Although the treatment for breast cancer still remains one of the most prevalent causes of morbidity and mortality resulting from cancer world over with huge global burden [1,2]. It is the leading the new cancer cases in women (about 25 %). In spite of the improvements in early diagnosis and treatment of the disease, breast cancer remains a problem in the management of as well as the survival outcome of patients [3]. The disease is heterogenous, different subtypes of the disease with different biological features, response to treatment, and prognosis. Among the identified subtypes, hormone receptor-positive (HR +), human epidermal growth factor adopt (HER2 +), triple-negative breast cancer (TNBC) is the most common. It is the aggressive nature of TNBC, as indicated by its poor prognosis and scarcity of targeted therapies, which makes it a prime target for new more successful treatment development [4,5]. The contemporary breast cancer treatment combines surgery, chemotherapy, radiation therapy and hormone therapy for different type and stage of malignancies. Although conventional therapies have markedly increased survival and quality of life in numerous patients, they continue to have certain limitations, i.e., adverse side effects, recurrence, and treatment resistance [6,7]. Chemotherapy, for instance, takes advantage of fast dividing cells, but it does harm to healthy cells thus causing such side effects as fatigue, loss of hair and loss of the immune system. Radiation therapy despite being effective in destroying

* Corresponding authors: School of Pharmaceutical Sciences, Vels Institute of Science, Technology & Advanced Studies, Pallavaram, Chennai, Tamilnadu 600117, India.

E-mail addresses: sumampharmacy@gmail.com (K. Sumalatha), tpsphc@gmail.com (P. Theivendren), drgmathipharm2017@gmail.com (G. Rathinasamy).

https://doi.org/10.1016/j.insi.2025.100054
3050-7871/

localized cancer cells can damage body tissues causing complication in neighboring Tissues. In addition, patients suffering from metastatic or resistant types of breast cancers are not likely to respond optimally to conventional therapies, re-emphasizing the need for alternative therapies with lower morbidity and improved long term outcomes [8,9].

Preventing and treating breast cancer benefits greatly from natural products studied through the years. Natural compounds are recognized as a promising approach because they can regulate distinct cellular paths of cancer initiation, promotion, and metastasis. These comprise; antioxidant action, anti-inflammatory effects, regulation of cell proliferation, apoptosis and angiogenesis [8,10,11]. In addition, several natural compounds are thought to possess multiple-targeted mechanism, which increases the therapeutic value of such compounds and decreases the probability for becoming resistant. The mechanisms of the natural products in cancer cells are not restricted by their direct cytotoxic activity. Several compounds isolated from plants have been found to control important proteins which promote cancer progression, such as the renin complex and nuclear factor-kappa B (NF-κB), and a transcription factor that controls inflammation and cell survival [6,10,12]. While the promising findings portend well for expecting new treatments from natural products, problems still exist in terms of taking potential of natural products to be clinical therapies. Beta-carotene, an antioxidant that is naturally occurring in the brightly colored fruits and vegetable like carrots, sweet potatoes and spinach, has been known to provide some benefit to health. As a precursor of vitamin A, beta-carotene is important in maintaining many body functions, including sight, immunity and the skin. But its role in cancer prevention and treatment especially breast cancer has generated increasing interest [13–17].

Anti-cancer properties of beta-carotene are thought to exist because of its potent antioxidant action. Protecting the cells from DNA damage that may occasion cancer, beta-carotene scavenges free radicals and curbs oxidative stress. In addition, beta-carotene has been found to modulate cell cycle regulation favouring cell's differentiation and arresting the uncontrolled cell multiplication seen in cancer. Research shows that Beta-carotene can trigger apoptosis in cancer cells, particularly in breast cancer, trough activation of important apoptotic pathways [18–20]. In addition, they found beta- carotene to modulate vital signaling pathways that take place in the process of cancer progression. For instance, it is capable of down regulating the expression of genes governing tumor metastasis, matrix metalloproteinases (MMPs) which are responsible for the degradation of the extracellular matrix and the invasion of the tissue [21,22]. This work aims to study the possible role of beta-carotene as a potent therapeutic agent in aiding in the treatment of breast cancer; determining its mechanisms at the molecular level; its antioxidant, anti-inflammatory and apoptotic effects; and to evaluate its potential

Materials and methods

Network pharmacology

In the first place, data is retrieved through searching for Beta-Carotene targets in databases such as Swiss Target Prediction or STITCH, and retrieving Breast Cancer targets at platforms such as DisGeNET. The processed data are then analysed to find out the common and unique targets which are presented in a Venn diagram using such tools as Bio Venn to explain the intersection and differential targets in integrated networks between Beta-Carotene and breast cancer pathways, if any present or absent. Analysis of structural and functional properties of Beta-Carotene is carried out on visualization software such as Chem Draw or PyMOL while target classes are determined and classified using Swiss ADME, a similar platform. A program, like Cytoscape or STRING, will generate a molecular network browsed around PARP1 and delineated with downstream interactions for oncogenic pathways [23,24].

Ramachandran plot statistics

For the assessment of protein quality with regard to its secondary and tertiary structures, we employ the PDBsum PROCHECK summary from the European Bioinformatics Institute (EBI). The output from PROCHECK provides protein 5LX6 data on stereochemistry with Ramachandran statistics plotting the percentage of residues located in: G-factors are used to test the reliability of dihedral angles and the fundamental covalent parameters of the chain. Moreover, ensure bond lengths and bond angles, as well as check residues that fall out of normal ranges for structural analysis. It is necessary to compare this information with existing experimental results, because this step guarantees that the model can be trusted for further computational or experimental studies [24,25].

Molecular docking studies

Key procedures involved in Auto-Dock Vina-based protein-ligand docking are as follows. In order to prepare a 5LX6 protein structure, we removed water molecules and added polar hydrogen atoms. Then create the ligand file containing the necessary 3D structures and rotatable bonds. Set up the docking grid box with a large core around the X, Y, and Z binding pocket. Then import the protein and ligand files into POAP and then set the docking parameters. Run Auto-Dock Vina to do the docking simulations. Analysis the simulation results and determine binding affinity, as well as visualize the ligand position in the binding site of the protein [26–28].

Molecular dynamics studies

Desmond was used in the MD studies, where the protein-ligand complex was prepared and the simulations set up in an explicit solvent model (including a TIP3P water box, and addition of ions to maintain neutral charge, by adding water molecules). Simulation conditions are devised, such as those for boundary conditions and periodic boundary condition with details defined in temperature, pressure, and time-step (generally starting with energy minimization step). Start the MD simulation, and then use it to run over a chosen NPT ensemble. We proceeded to analyze the trajectory data after the simulation to determine RMSD, RMSF and continuous interactions between the protein and ligand [26–28].

ADMET studies

Computational methodologies were applied to appraise ADMET characteristics of Beta Carotene, these include physicochemical, pharmacokinetic, and druglike properties. The SMILES string is used to show the molecular structure. These important descriptors, such as molecular weight, hydrogen bond acceptor/donor, topological polar surface area (TPSA), and lipophilicity (log P values), were calculated. The analysis included pharmacokinetic properties like GI absorption and blood brain barrier permeability and CYP enzyme inhibition. To measure Beta-Carotene's drug-likeness, LiPinski, Ghose, Veber, and other filters were used. After this, we evaluated the structure for potential medicinal chemistry problems, like PAINS and Brenk alerts. In order to estimate the measures of probability of progress to the clinical application, scientists determined the values of bioavailability and synthetic accessibility [26–28].

Density functionality theory

The .sdp files which scientists obtained from the public database of PubChem belonged to the specific chemical compound; Beta-Carotene. Using the Spartan14 interface, researchers imported files and performed steps meant to reduce energy consumption. Investigators used

GaussView 6.0.16 to determine Hatree energy levels for the HOMO and LUMO orbitals of the compound. The process is making a conversion of HOMO-LUMO energy gap values from Hatree energy to electron-volt energy units. Interactions between the energy bands for Beta-Carotene is critical to stability analysis [26–28].

Formulation of Beta-Carotene-encapsulated SLNs

Beta-Carotene was incorporated into SLNs by employing oil-in-water microemulsion technique by utilizing high-speed mixing and ultrasonic treatment. To prepare the referred lipid mixture, 5 mL of ethanol was mixed with 2 g of cetyl palmitate and kept in a water bath at a temperature about 5–10 ˚C above its melting point (54 ˚C). By combining the heated solution, it made it possible to form a homogeneous liquid phase. After the lipid mixture had melted, 5 mg of Beta-Carotene was allowed to be exposed to sonication for 1–2 min. The Ultra Turrax T25 homogenizer from IKA incorporated the lipid solution sheared for 2 h up to 3000 rpm on a continuous basis in to 50 The ultimate conclusion on the Method resulted in a transparent microemulsion. In India, the microemulsion was introduced to an instrument in the REMI laboratory and spun for 30 min at 10,000 rpm [29–31].

Entrapment evolves and drug load capacity of Beta-Carotene-encapsulated SLNs

The analysis of Beta-Carotene entrapment inside SLNs involved dissolving 5 mg of SLN particles with 10 mL of methanol then performing centrifugation at 10,000 rpms for 30 min. Laboratory testing of Beta-Carotene concentration occurred through evaluation of the supernatant solution samples [29–31]. Laboratory staff analyzed the drug loading capacity and entrapment efficiency of Beta-Carotene-containing SLNs through equations (1˚ and 2).

$$\%EE = [\text{Totalamountofadded} - \text{freeBeta} - \text{CaroteneofBeta} - \text{Carotene}/\text{Total}$$
$$\text{Beta} - \text{Carotene}] \times 100$$

$$\%DLC = [\text{TotalamountofBeta} - \text{Caroteneadded} - \text{freeBeta} - \text{Carotene}/\text{Weigh}$$

In vitro drug release of Beta-Carotene-encapsulated SLNs

By using in vitro dialysis bag diffusion analysis, we sought to describe how Beta-Carotene exited Beta-Carotene-encapsulated-SLNs. To initiate the dialysis experiments, it was necessary to load a dialysis membrane with a cut-off size of 3500 Da with 5 mL buffer solution and to add 50 mg of Beta-Carotene-encapsulated SLNs. A 100-mL buffer solution at 0.01 M acetate buffer and pH 5.5 was used as a receiving container whereas separate 0.01 M phosphate buffer pH 7.4 was used for collecting. Operation at room temperature was maintained by having the shaker at a speed of 100 rpm. As the SLNs released Beta-Carotene, the new standard medium came into introduction in the buffer solution of the external compartment. In this study, the whole range of liquid samples was treated by methanol [29–31]. Beta-Carotene material was separated by centrifuging at 25 ˚C; 14,000 g of force were used. The researchers used the HPLC analysis technique to find out the concentration Beta-Carotene released.

Drug release kinetics of Beta-Carotene-encapsulated SLNs

In vitro experiments results supported the determination of Beta-Carotene drug release kinetics and diffusion properties from SLNs. The research used five kinetic models for analysis, i.e., zero-order and first-order, Higuchi, the Korsmeyer-Peppas, and Hixson-Crowell dynamics. Depending on the chosen model mechanisms different release patterns from SLNs are observed [29–31].

Stability studies of Beta-Carotene-encapsulated SLNs

Various physiological media were tested for the stability of newly developed Beta-Carotene-encapsulated SLNs, including 10 % NaCl, 0.5 % BSA, acetate buffer (pH 3.5 and 5.5), phosphate buffer (pH 7.5 and 9.0), and simulated gastric juice. 100 μL of the freshly prepared Beta-Carotene-loaded SLNs microemulsion was added to each of the 0.5 mL of physiological mediums and incubated at 37 ± 2 ˚C The UV–visible spectrophotometer examined the maximum absorption (λ_{max}) from the samples by performing readings after vortex mixing and during specified time periods of dynamic measurements [29–31].

LC-MS analysis of Beta-Carotene-encapsulated SLNs

Shimadzu LC-MS system was used in the evaluation of Beta-Carotene-encapsulated SLNs. The testing system sampled a minute portion for analysis by using water and methanol in its mobile phase. Two distinct strategies were used in the separation operation by the analysis system in order to identify compounds with two observed ionisation states. Results of run times and mass spectra of bioactive molecules were used to show buffering of active constituents. Because the individual molecular ions were efficiently identified through the chromatographic analysis, there has been proof of successful encapsulation technique as well as strong stability for the bioactive compounds [29–31].

FE-SEM analysis of Beta-Carotene-encapsulated SLNs

Morphology of Beta-Carotene-encapsulated SLNs was studied using FE-SEM. The lab technicians dissolved 2 mg of freeze-dried Beta-Carotene-encapsulated SLNs in 1 mL distilled water and pipet 2 μL of the mixture on glass for examination. When the Beta-Carotene-SLN layer is dried, a small amount was spread on a Glass surface for additional observation [29–31].

FTIR analysis of Beta-Carotene-encapsulated SLNs

The beta-carotene encapsulated SLNs analysed through FTIR, and it could estimate particle crystallinity using the under FE-SEM (JEOL JS-M6700). Preparation of a 2 mg dosage of the lyophilized SLN in water allowed further characterization and measurement using gold-coated plating. It was shown that the protocols of the pellets exhibited contemporary pharmaceutic properties such as safe encapsulation efficiency, stability, and successful nanoparticle characterization [29–31].

MTT assay

MCF-7 cells achieved confluency in DMEM supplemented with 10 % FBS and antibiotics (100 IU/mL penicillin and 100 μg/mL streptomycin) under the condition of an environment of 5 % CO2 at 37 ˚C with humidity. For dilution of the pellet cells (1.0 × 105 cells / mL), aliquots of 100 μL were then spread onto 96-well plates. The cells were exposed to the sample compounds after a 24 h incubation prior to subsequent incubation until the MTT assay was started. A microplate reader was used to determine the 570 nm absorbance for viability assessment [26–28].

Results and discussion

Network analysis

An interaction network diagram presented here shows complex relationships between major oncogenes, tumor suppressor genes, and DNA repair genes, highlighting their applicability to PARP (poly ADP-ribose polymerase). >60 genes are portrayed as being integral to a complex molecular architecture, in which PARP acts as a major node in a very

tight network, reflecting its central role in repair of DNA- as well as cellular stability. Representative cancer associated genes such as TP53, BRCA1, BRCA2, CDKN2A, and RAD51 that are critical for DNA damage repair and cell cycle control are integrated into this interlinking model with their role and interactions with PARP highlighted. BRCA1 and whether BRCA2 constitute important elements of homologous recombination repair have high interactions with PARP which further establishes that the synthetic lethality effect is seen in BRCA-mutant cancers linked with PARP inhibition. The presence of such genes as TP53 and MYC that are fundamental for the regulation of a cell cycle and apoptosis has shown the major implications of PARP signaling in oncogenesis. The presence of such receptors as ERBB2, transcription regulators such as STAT3 and JUN, as well as such genes as RAD51 and MSH2 in the network suggests that blocking PARP based inhibition can have implications on a variety of pathways in cancer biology. The wide links of network connections prove the active communication between these genes, which proves the complexity and interaction of the underlying regulatory processes. This wide connectivity in network provides useful insight that may inform the development of combination therapy approaches involving PARP inhibitors combined with agents that target co-expressed or co-regulated genes. Such analysis highlights how systems biology is useful in identifying the critical molecular targets for cancer treatment Fig. 1.

Protein analysis

The PROCHECK analysis results revealed positive structural features for the protein especially on its Ramachandran plot data statistics. Out of the 380 residues 298 are found in regions A, B and L that meets or exceeds the 90 % limit as by definition they are in the regions that are most favored regions in Ramachandran Plot regions. With the best configuration, the backbone achieves greater stability. The 8.5 % residues consisting of 28 residues are found in the additional allowed regions (a, b, l, p), and about 0.6 % of these (two in total) residues are found in the generously allowed regions (~a, ~b, ~l, ~p). The structural qualities of the protein model are outstanding since its all residues are placed in allowed regions. The organization of the model's structure is good, none of the model's residues falls out of the allowed regions. In such a configuration, glycine and proline residues tend to enhance structural stability through the formation of flexible segments that stabilize the protein backbone.

Analysis of G-factor allows the researchers to measure the quality of protein, comparing dihedral angles and covalent bond parameters at once. Phi-Psi distribution score of −0.18 verifies correct positioning of backbone angles as the model shows little deviation from the norm. The Chi1-Chi2 (0.17) and Chi 1 only distribution (0.19) values show that the lesser steric clashes among side chains have been brought out. The confirmation that the peptide bond does not have any trans-*cis* bond arrangement abnormalities is provided by the omega value of 0.00. The values for main chain bond lengths follow what is regarded as allowable variation patterns (0.15), and comparable insignificant changes

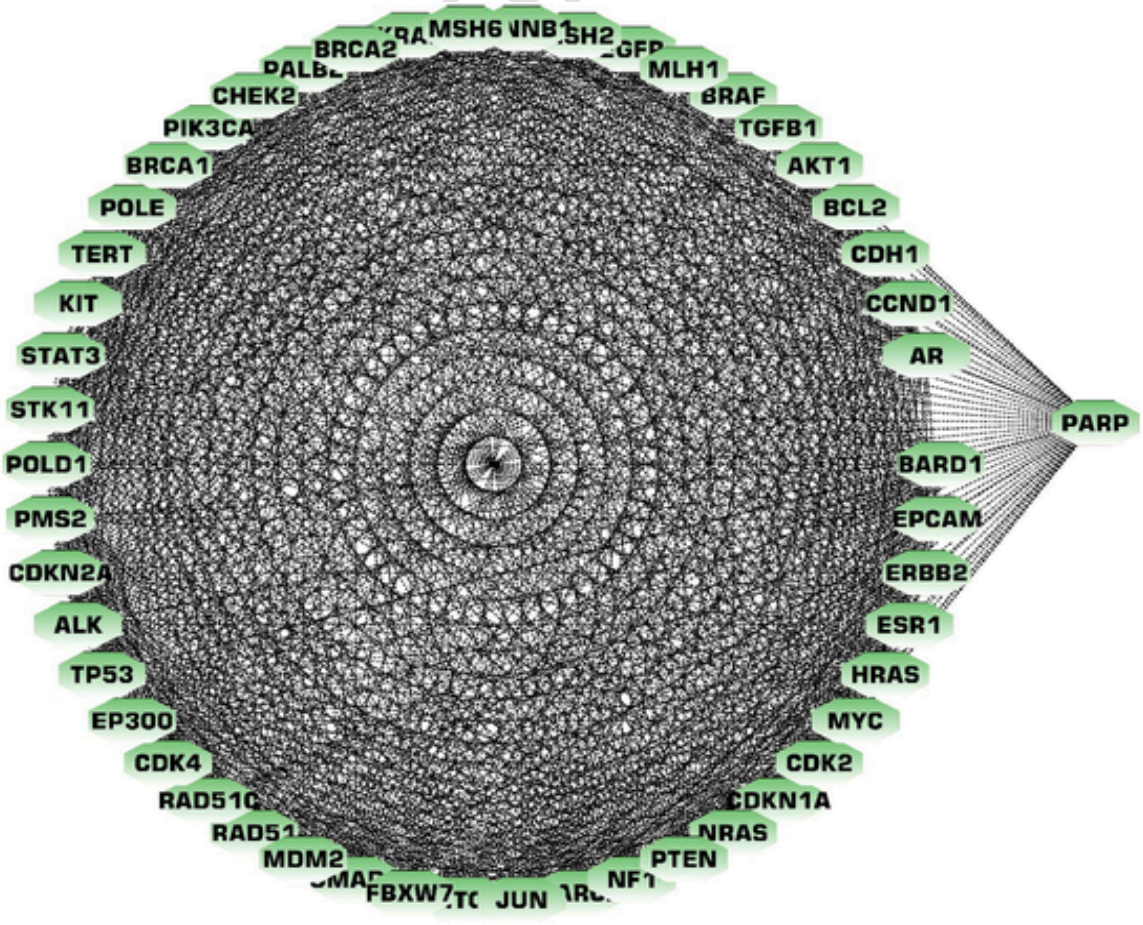

Fig. 1. Protein-protein interaction (PPI) network showing PARP as a central hub connected to multiple cancer-associated genes, highlighting dense molecular interactions relevant to DNA repair, cell cycle regulation, and oncogenesis.

exist for the measurements of bond angles (0.21). The finding of the G-factor value of 0.10 from the model confirms that the structural characteristics are common and evenly distributed. The protein has superior quality characteristics since its geometric measures, and equilibrium match up with the conventional standards without significant deviations. The accurate structural stability allows for efficient probe of protein interaction in chemical events.

Secondary structure elements include H1-H7 α-helices, β-strands and unidentified loops. Healthy decomposition of amino acids in the given sequence enables us to determine the place of a secondary structure in the protein. α-helices, and new sheets constitute major parts of segments of the structure where the amino acid sequence underlies as essential structural building blocks. Some protein residues are highlighted to show related secondary structure annotations while explaining functional characteristics and orders of structural elements in the protein. Reliance on these particular domains ensures not only fundamental structural support but also the efficacy of the protein in mediating biomolecular interactions with additional ligand. The identified structural elements improve the capability of researchers to examine proteins with regards to their dynamic interaction with their binding partners.

Ligand-binding is present at specific locations on the protein, with hydrogen bonds provided by green dashed lines extending 2.84 Å and 2.96 Å to attach Ser 927 and Gly 888. The residues Tyr 932, His 887, and Ala 911 are of vital importance for the binding interaction maintaining as the prerequisites for the binding interaction via π-stacking and hydrophobic connections. Such interactions promote enhanced ligand targeting and increased binding affinity to the protein of interest.

Structural specifics are shown in the database with the help of the cleft sizes of protein, cleft connections with ligands and exposed areas. Reply by demonstrating differences in exposed and hidden vertex numbers this table indicates how these characteristics influence the frequency of clefts interacting with ligands. Cleft 1 is an important binding region since it has 72.43 accessible surface areas and 14.86 buried sites. Cleft residues form interactions with each other to provide binding site for ligands 78P 1101 [A] and 78P 1101 [B]. The depths of the clefts provide insight into the nature of their architecture and their tendency to bind ligands. Scientific examination of all the clefts will allow researchers to find primary binding zones, thus improving our understanding of protein –ligand interactions Fig. 2.

Molecular docking analysis

Beta-Carotene and Myricetin exhibited the highest binding affinities towards the target protein, since their scores were –10.0, implying efficient protein interaction. Lutein's docking score of –9.9 confirms the discovery that carotenoids in combination with plant sterols expressed emancipated positive scoring patterns during the analysis. Other complex structures of lipophilic compounds such as beta-Apo-8-carotenal (–9.3) and Lutein56-epoxide (–9.1) participate in probable molecular recognition, among other important compounds. The potential of flavonoids is revealed through the three compounds Luteolin, Quercetin, and Apigenin, which exhibit docking affinities from –8.6 –8.8, which is indicative on their biological importance. Once doped with lots of hydroxyl groups of polyphenols will bind well because of hydrogen bonds and π-π interactions that will result. Detected from the screening, were simple aliphatic and sulfur-containing isothiocyanates compounds Dimethyltrisulfide and Dimethyldisulfide with scores between –2.3 and –2.6, indicating low binding affinity. The range of docking scores suggests that ligand-protein binding is to a large extent dictated by the molecular composition and functional chemical groups found in the ligands. The results indicate that carotenoids and flavonoids are indeed a good prospect for further in vitro testing, as the outstanding docking performance of the compounds and their recognized biological significance should not be overlooked. Key information from the results and molecular binding site assessment of the three protein-ligand complexes provides important details regarding the ligand-protein interactions. The Protein –Ligand Interaction Profiler (PLIP) was used to analyze the three systems: myricetin complex, lutein complex, and beta–carotene complex.

Beta-Carotene complex

In the beta-carotene complex analysis, it was shown that stability is achieved through the hydrophobic interactions of Thr 890, Ala 893, and Ile 897. The ligand hydrogen bonding with Tyr886 and Arg931 supports the reinforcement of stability and the specificity of the binding site. Stable interactions between protein and ligand atoms affirmed at between 3.28 - 3.98 Å could improve effectiveness of therapeutic interventions.

Results of binding site analysis demonstrate that ligand molecules consistently make stable favorable interactions with vital protein residues in all complexed systems examined. The combined data becomes a foundation for developing new molecular structures, which can either augment or blunt protein activity in medical uses. For validation and elucidation of the application of these interactions in therapeutics purposes, it is recommended that we conduct molecular dynamics studies along with in vitro binding tests Fig. 3.

Myricetin complex

The myricetin molecules are bonded to each other by the protein to create vital hydrophobic and hydrogen bonding with the observed structure and corresponding PLIP table. Triplet hydrophobic bonds re-

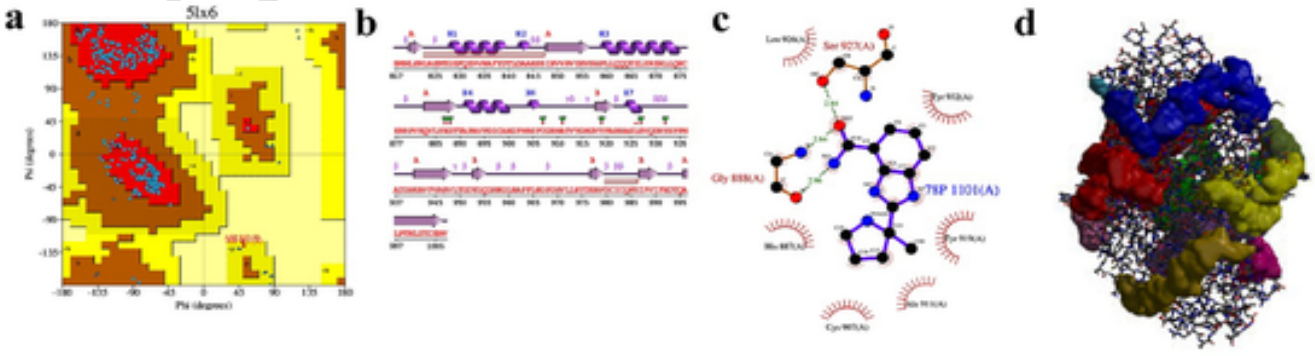

Fig. 2. Structural analysis of protein-ligand complex: (a) Ramachandran plot, (b) secondary structure prediction, (c) 2D interaction map with key residues, and (d) 3D surface representation of molecular docking pose.

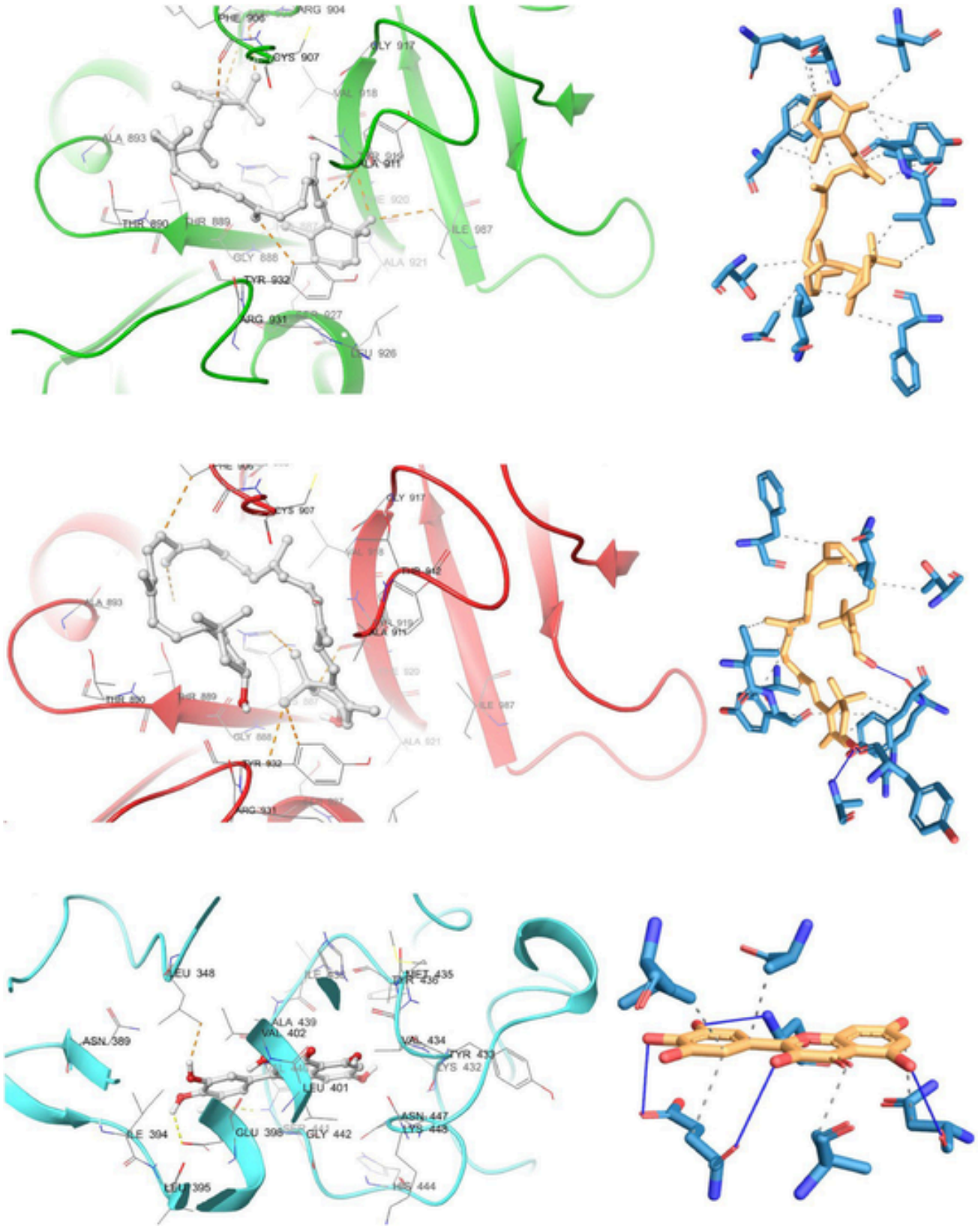

Fig. 3. Molecular docking interaction of β-carotene, lutein and myricetin with the target protein 5LX6, illustrating its binding orientation and key stabilizing interactions within the active site, including hydrogen bonding and hydrophobic contacts.

sult from the interaction with Leu348, Glu398, Leu401, Ala439 and Asn447. These specific residues in the target protein are mutually critical to its affinity and ligand selectivity. Interaction stability of the complex is predominantly supported by hydrogen bonds that involve Glu398, Glu399, Ser441, and Asn447. The dual protein-ligand interactions that take place at distances from 2.7 to 3.7 Å show powerful binding capacity of the ligand indicating the possibility for its use as an inhibitor. The hydrogen bond stability within the ligand and protein binding is reliable, and thus, having a stable binding matrix, scientists can tailor new therapeutic agents resistant to proteins with comparable architecture Fig. 3.

Lutein complex

Analysis of the lutein compound showed critical residues including Thr890, Ala893, Ile897, F906 and Val918, involved in hydrogen bonding and hydrophobic interactions over the range of 3.22–3.98 Å. Stability of the protein-ligand interaction relies on such important residues. The increased binding affinity of the ligand is due to hydrophobic contacts between 3.22 and 3.98 Å.

Hydrogen bonds between Tyr886 and Ala921 complemented by Arg931 strengthen specificity and ligand-receptor interaction stability. The strong bond structure of the complex is as a result of hydrogen bond distances varying from 2.5–3.2 Å. The drug-like complex is highly promising for further drug design studies owing to the dependence of diverse hydrogen bonds and hydrophobic interactions. Significant importance of both hydrophobic interactions and hydrogen bonds on the specificity of ligands with strong affinity binding is demonstrated with the aid of the PLIP analysis. The patterns of interaction revealed in myricetin, lutein and beta-carotene complexes correspond to the acknowledged antioxidant and anti-inflammatory activity of these ligands. This study identifies the vital role played by certain amino acid residues in stabilizing ligands and provides essential information for the design of very effective targeted compounds for these proteins. Employing state-of-the-art computational techniques together with the direct evaluation of the binding behavior, scientists will establish the exact therapeutic merit of these components Fig. 3.

Molecular dynamics analysis

5LX6_beta-Carotene complex

The interaction evaluation provided complete information about the stability of protein-ligand binding and their binding affinity. The RMSD values demonstrate consistent protein-ligand interactions over time since the protein backbone deviation and the ligand deviation fluctuate during the simulation. In the 100 ns simulation, the ligand always bound to the target protein through conformational modification of the target protein in the early stage, for which the stability was confirmed by keeping track of the RMSD fluctuation.

A state of fluctuation in RMSD values of both protein backbone and ligand is seen at the beginning of the simulation. At the 60 ns simulation time, the co-protein-ligand system attained equilibrium and by that time, researchers could therefore obtain trusted structural outcomes. Application of RMSF made evident increased flexibility for protein residues that are located in loops and binding sites. Increased flexibility is indicated by peaks in the RMSF plot at several residues, as a result of changes in the protein shape due to ligand binding. The presence of substantial flexibility at critical spots in the protein appears to be beneficial in terms of biological activity at ligand binding, as confirmed by this analysis.

Cleft statistics show that the ligand mainly interacts with the key residues that are located in the cleft, which confirms its ability to bind. The power of binding and the accuracy of the interaction are dictated by both the cleft area, and the residues involved in the cleft. All elements were confirmed to add to both functional and realistic features of the model through the G-Factor analysis using validation of proper covalent and dihedral angles and an overall G-factor score for predicted structures. Interactions fraction matrix analysis revealed that Leu 348, Val 402 and Tyr 438 are key players in frequent interactions with the ligand. Analysis of the interactions using bar graphs showed that during the course of the simulation, Gly 349 and Glu 406 were key ligand-interacting residues. The examination favors the idea that the indicated residues have essential importance in stabilizing ligand-protein interactions and could regulate functional activities. At the same time, analysis of the torsion angles showed that in the course of the simulation period, both the ligand and the protein maintained their structural stability. However, the torsion angles reported throughout the simulation did not change, indicating that the mode of binding was stable and no major conformational fluctuations were experienced after the ligand bound. The stability of the values throughout the trajectory supports the assertion that there has been a steady bound state of the protein-ligand complex during the simulation. The data suggest that there is a stable and long-lasting relationship between the ligand and protein and several residues in the complex are important for maintaining its structural and functional features. By using our simulation results we can show that the protein-ligand complex exhibits a stability that could be attractive as a target for further research and therapeutic use. These constructions reached the highest validation scores in the top 649 ranks for PROCHECK and G-factor –which reflects their better quality for future drug design studies Fig. 4.

5LX6_Lutein complex

The stability of the configured protein-ligand complex was measured using 100 nanosecond molecular dynamics simulation. The protein backbone and ligand dynamics were examined by using structural parameters such as RMSD, RMSF, protein-ligand contacts, and ligand's torsion flexibility.

From analysis of the RMSD plot it is evident that during the course of the simulation, protein and ligand remained stable. The stability of the atom Cα of the protein, backbone and that of the side chains were noted; and RMSD values just hovering around 1.5 B2.0 A pf post-10 ns (and toward the end) an indication of the calculated conformation of protein stability during the simulation. The RMSD analysis of the ligand against the protein uncovered fluctuations in the 2.0 to 3.0 Å region that showed that ligand within the binding site had undergone partial reorganisation, probably induced-fit or dynamism of near-by residues. On the other hand, the ligand had a relatively low RMSD when it was fitted on its own (1.0–1.5 Å), which meant that it remained internally conformationally stable as it accommodated new local positions.

In order to observe how the residues of the protein behaved, we used an RMSF analysis. Almost all residues fluctuated with values under 1.5 Å, this meant that the protein maintained its folded and stable structure during the simulation. Protein terminal and loop regions were found to have a clear peak in the RMSF curve, as expected. Mode analyzing intermediate fluctuations in binding-site residues showed that these regions were involved constantly with the ligand but kept their structural placements intact. To identify protein-ligand contact sites as primary interaction sites, protein-ligand contact analysis was performed using the trajectory. As shown in the interaction histogram, GLY888, PHE902, CYS907, VAL918, LEU926, ARG931, and TYR932 maintained a steady interaction with the ligand. Residues ARG931 and GLY888 interacted most often with the ligand meaning their possible role in keeping the ligand's position in the binding site. These residues promote hydrogen bonding with the ligand, provide hydrophobic contacts, or result in interactions with π-π stacking.

The findings were supported by the interaction trajectory confirming that the people held constant contacts during the simulation time. Engagement was maintained for the residues Val918, Arg931 while it

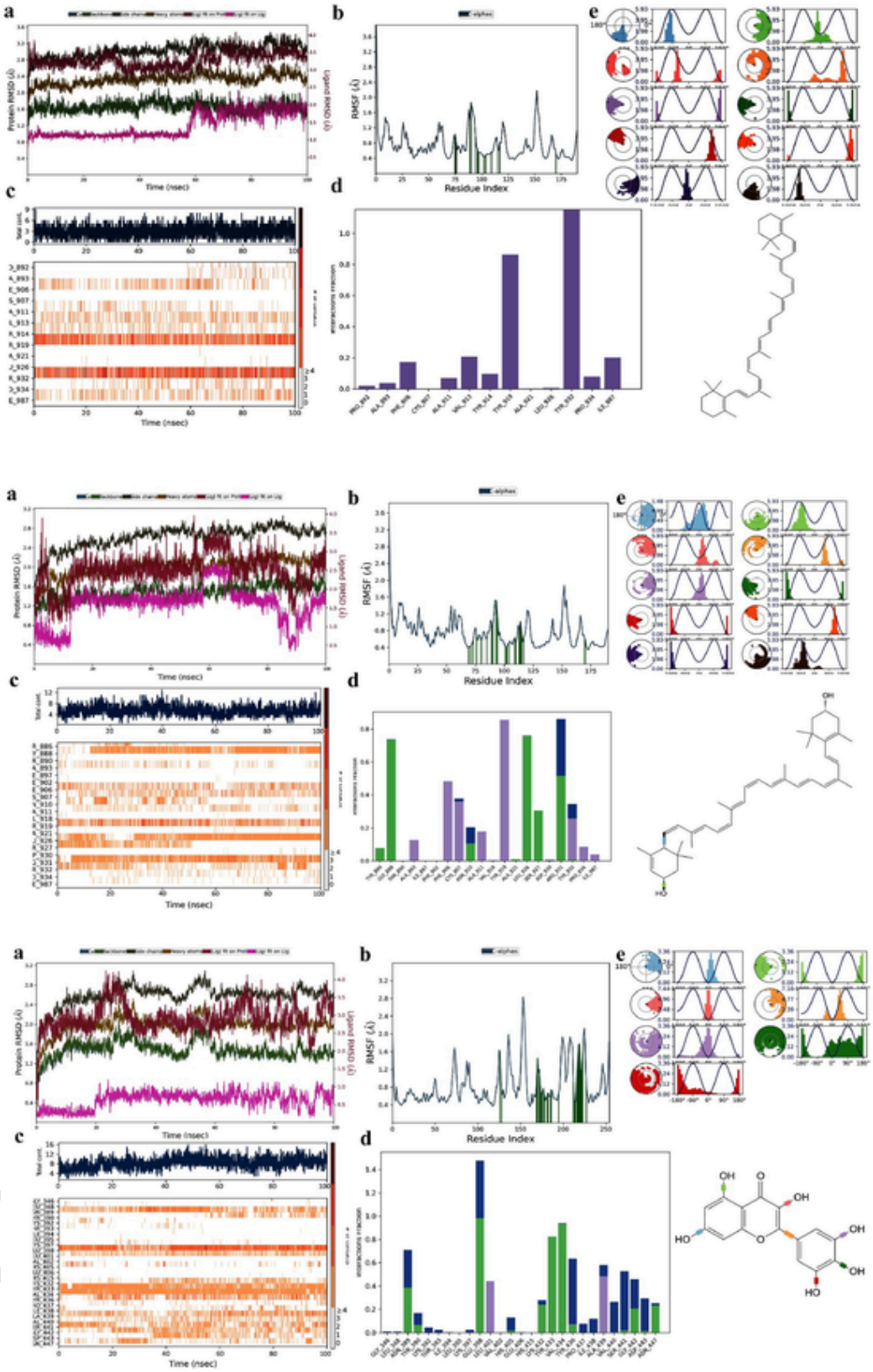

Fig. 4. Molecular dynamics simulation of 5LX6_β-carotene, lutein and myricetin complex showing RMSD (a), RMSF (b), hydrogen bond occupancy (c), key interacting residues (d), dihedral angle analysis (e), and β-carotene chemical structure.

was less persistent for interaction with Thr890 and Asp930. From this analysis we reveal a tightly defined binding face, both strong and subtle integrated interactions to define binding specificity and affinity.

Since the ligand's torsional properties were considered in the analysis of the ligand, it was revealing that its dihedral angles exhibited constrained motions in accord with the fact that the ligand assumed a stable bound structure. Clear peaks are seen in the torsional profiles indicating the existence of preferred dihedral populations. This degree of restraint is in agreement with the ligand's hard hold on the binding site, placing it in a holding spot which maximizes efficient binding. In conclusion, the molecular dynamics simulations show that the protein-ligand complex preserves its structural stability, with critical residue interactions remaining stable and with extremely weak conformational changes in the ligand. With low RMSD values for proteins and ligands, similar residue interactions, and limited torsional angles, the stability of the protein-ligand binding mode is confirmed by experimental analysis and free energy calculations Fig. 4.

5LX6_Myricetin complex

MD simulations over a 100 ns trajectory were used to analyse the protein-ligand complex, explore structural stability, residue flexibility, ligand conformation alterations, and atomic-level interaction dynamics. Since the analysis started with RMSD, as demonstrated in the first graphic, it was clear that various areas of the protein and ligand behaved differently. RMSD stabilization for Cα and backbone proteins atoms at approximately 1.5 Å and approximately 1.6 Å after 10 ns indicates overall stability of the protein throughout the simulation. Slightly higher fluctuations for side chains and heavy atoms were seen, the stabilised RMSDs were approximately 2.7 Å and 2.0 Å, respectively. Ligand alignment to the protein through RMSD brought out fluctuations within 2.5–3.5 Å, indicating moderate flexibility to the binding site. In contrast, the ligand RMSD stayed under 1.0 Å when matched to its own structure, meaning even as the ligand assumed motion during its tours within the binding site, its intrinsic conformation was maintained.

RMSF analysis, interpreted residue flexibility. Most residues were found to be flexible in their small range of 0.5–1.0 Å, suggesting an overall stable protein structure. Residues 85, 150 and 200 (at ~ > 2.0 Å), where the peaks are localized, signify that the protein has flexible, or potentially solvent exposed regions or loops. Results from RMSF plot stating that the green bars indicate that receptors with low flexibility may complicate the interactions between ligands in making them stable. Interaction profiling recognizes that LEU401, GLU398, TYR434, and VAL440 are involved in ligand binding with LEU401 being most involved and probably involving hydrophobic and van der Waals interactions. The uniform AP distribution across the binding domain validates the complementary nature of interaction between the ligand and the candidate receptor in our model.

Our ability to visualize interaction timeline by means of heatmap allowed us to monitor protein-ligand contacts throughout time. Residues such as GLU398, TYR434 and VAL 440 were primarily bound throughout the 100 ns simulation indicating that they may serve to anchor the receptor. Remainder of these contacts stabilises ligand in the active site, which is consistent with a steady ligand RMSD (self-aligned). Also, visual inspection of the upper panel shows fluctuations in the contact numbers between 5 –15, which supports the observation that binding did not change at all during the simulation. The viewing of ligand torsions served to elucidate the dynamics of rotatable pieces as they were different in 3D conformations. Normal distribution of most torsional angles with respect to central optimal dihedral angles offered support for the rigid nature of the ligand and the lack of internal stress during the course of the simulation. The torsions demonstrated a flat range of motion which justified the conclusion of RMSD analysis that the ligand maintained good conformer stability through the simulation with polar plots being another confirmation. All these results identify a combined effect of showing that protein-ligand complex has a stable structure as key residues during the simulation still remain in contact with the ligand. The rigidity of the ligand implies that it possesses a proper, and stable, binding affinity to the pocket. The confirmation of the stability of the ligand by these results justifies its use as a stable binding molecule and leads to potential drug development or optimization work Fig. 4.

ADMET analysis

The present study examined Beta Carotene, Lutein, and Myricetin, as the worm potential therapeutic compounds using the SwissADME tool to evaluate their drug-likeness, bioavailability and membrane permeability across the blood brain and intestinal restriction. The qualitative analysis of predicted HIA, BBB permeability and P-gp interaction (a recognized efflux transporter) was performed using the Boiled-Egg model. On the Boiled-Egg plot, and LogP and pKa predictions, Myricetin seems to be located outside the predicted boundaries for HIA and BBB permeability, hence having high potentials for poor passive gastric absorption while having a very low chance for BBB permeability. According to this, its TPSA value of 151.59 $Å^2$ is greater than the normal threshold of 140 $Å^2$ that has been generally accepted to be required for good permeability. Moreover, the structural characteristics of Myricetin, for example, its six hydrogen bond donors, and eight hydrogen bonds, acceptors are unfavourable to its membrane permeability. Based on the prediction and drug-like indices (Veber, Egan and Muegge), the compound appears to be a non-substrate for P-gp, and has failed several drug-likeness tests, thereby indicating that oral bioavailability will be limited even with the potential therapeutic application. Further, this low GI absorption prediction is consistent with the Boiled-Egg model, which supports the difficulties in delivering Myricetin with traditional oral regimens unless improving uptake is possible by means of nanocarriers and prodrugs at use.

Meanwhile, the TPSA of Lutein is much lower at 40.46 Å2 and therefore falls within the range considered suitable for absorption. Its pharmacokinetic profile is favorable with 10 rotatable bonds and only 2 hydrogen bond acceptors. Moreover, Lutein does not belong to the BBB or HIA regions according to Boiled-Egg modeling which may suggest the possible limits to its absorption and reaching the brain. Poor aqueous solubility and increased metabolic instability results from the high lipophilicity (WLOGP = 10.40) paired with the high molecular weight (568.87 g/mol). SwissADME categorizes Lutein as a possible substrate of the P-gp transporters with reflux occurring from routing its intestinal uptake, thus resulting in a reduced systemic intake. Lutein is not connected to PAINS or Brenk alerts, which means there are no naughty structural substructures in Lutein to give false positives in assays, apart from a single Lipinski violation likely due to its size. The bioavailability is not evaluated, and the synthetically accessible level is of medium.

Beta Carotene with WLOGP equal to 12.61 has an extremely low TPSA (0.00 $Å^2$), it lacks hydrogen bond donors and acceptors, which is a direct consequence of its absence of polarity. Indeed, while its lipophilicity is expected to aid membrane permeability, the large size and large logP values are likely to impair solubility and distribution of the compound. As to Beta Carotene, it is well worth noting that it is not pected to penetrate the BBB, and highly GI-absorbable compounds, like the one under investigation, are usually not included in the HIA and BBB-related models. Compared to Lutein it is a substrate for P-gp transport, which might have effects on bioavailability. Despite the fact that its physical and chemical characteristics comply with Lipinski's rules on hydrogen binding and rotatable bonds based on small size and relative lipophilicity, one can exceed the latter two properties over standard MW levels seen among druglike compounds. Passes all non-drug-likeness filters (Ghose, Veber, Egan, and Muegge); There is insufficient information on these compounds' water solubility data, and their un-

favourable GI properties indicate that they may not be easy to use therapeutically.

Overall, the physicochemical properties of all the three compounds studied in the present investigation do not correspond to the optimal requirements for the high gastrointestinal absorption and blood-brain barrier permeability indicated in the Boiled-Egg diagram. This highlights a key issue with orally bioavailable CNS-targeting agents that do not involve any structural modification or high formulation technique. In spite of their established effects as antioxidants and chemo preventive agents, the next generation of these phytochemicals must be optimized for delivery dosage forms, such as liposomes, polymeric nanoparticles, or synthetic modification, in order to maximize systemic uptake. Therefore, the researchers state that these natural compounds have desirable medicinal chemistry properties (with no significant PAINS or toxicophores), but their intestinal uptake is inconclusive and would probably require a creative delivery method for optimal therapeutic utilization Fig. 5.

DFT analysis

The HOMO and LUMO energies in Hatree and in electron volts and the calculated energy gaps for the Beta Carotene, Lutein, Myricetin, as representative antioxidants. The calculated LUMO and HOMO energy (gap) level spread in eV is an important metric that characterizes a molecule's electronic traits and possibly its reactivity with other molecules. Beta Carotene exhibited the highest HOMO energy (−9.2856 eV) and the lowest LUMO energy (−5.8330 eV), which is the largest energy gap of all compounds (−3.4526 eV). The larger the distance, the more likely the chemical tends to be stable with diminished reactivity under a normal system. This result is congruent with Beta Carotene's known antioxidant abilities, because it can be a successful scavenger of free radicals with minimal changes to its structure. Lutein showed an HOMO energy of −9.1245 eV and LUMO energy value as −5.9329 eV which would give an energy gap of −3.1916 eV. Lutein's HOMO energy was only marginally lower than the Beta Carotene's, but it possessed a substantially more negative LUMO, suggesting greater electron acceptance and probably superiority in redox behavior. Myricetin had the most negative (HOMO, −9.0143 e V) and the LUMO (−5.8374 e V) with an energy gap of −3.1769 e V. The reduced energy gap of Myricetin versus Beta Carotene indicates higher reactivity and in turn its capacity for ROS interaction, in line with its established antioxidant function. All in all, even though Beta Carotene still proves stable, Myricetin and Lutein are able to provide an improved level of electron-donating and antioxidative resiliency due to their lowered HOMO-LUMO energy deficits Fig. 5.

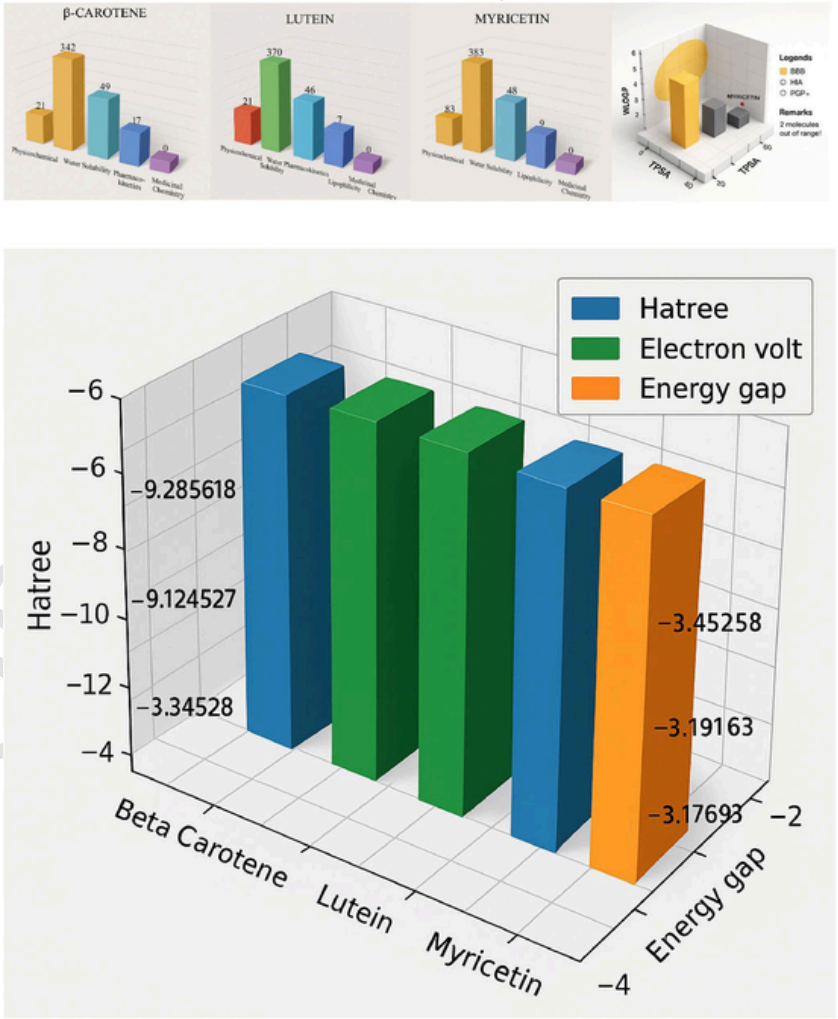

Fig. 5. Comparative 3D bar chart of β-carotene, lutein, and myricetin showing their physicochemical, solubility, pharmacokinetic, and medicinal chemistry profiles, alongside BBB permeability and TPSA-WLOGP plot and 3D bar chart comparing HOMO-LUMO energy values in Hatree, electron volts, and energy gaps for Beta Carotene, Lutein, and Myricetin, highlighting antioxidant molecular stability.

Beta-Carotene-encapsulated SLNs

The preparation of Beta-Carotene-encapsulated SLNs followed an oil-in-water microemulsion method. The Beta-Carotene encapsulation within SLNs reached 84 ± 1.12 % efficiency and achieved an 8.47 ± 0.93 % loading capacity Fig. 6.

In vitro release of Beta-Carotene from SLNs

The in vitro release study of Beta-Carotene from Beta-Carotene-encapsulated SLNs was performed in two buffer solutions (pH 5.2 acetate buffer, pH 7.5 phosphate buffer) at 35 ˚C through HPLC analysis. The research findings demonstrated that Beta-Carotene released into blood in a slow manner independent of Beta-Carotene-encapsulated SLNs. SLNs allowed 40.213 ± 0.412 % Beta-Carotene release when immersed in pH 5.2 buffer at 5 h. The SLNs also released 27.112 ± 0.012 % Beta-Carotene at 5 h when maintained in the pH 7.5 buffer. SLNs release Beta-Carotene more easily through acetate buffer solution (pH 5.2) instead of phosphate buffer solution (pH 7.5). The release of Beta-Carotene from Beta-Carotene-encapsulated SLN achieved maximum levels in all test buffered media during a 76-hour period. Test results demonstrated that the highest release of Beta-Carotene occurred at pH 7.5 where 85.119 ± 0.121 % was detected alongside an identical value of 82.121 ± 0.723 % obtained from pH 5.2 Fig. 7.

Drug release kinetics of Beta-Carotene-encapsulated SLNs

This study's reported data involved Beta-Carotene release. The examined drug release kinetics of Beta-Carotene encapsulated in SLNs through five basic model analyses (zero order, first order, Higuchi, Korsmeyer-Peppas and Hixson-Crowell model). The drug release kinetics that ran under controlled conditions are depicted in Fig. 8. Statistical methods were employed to predict the release rate constant together with the regression coefficient (r2) for each kinetic model. The extent of variable relationship strength increases when the r2 value moves toward its maximum value of 1. First-order kinetics results showed correlation values of r2 between 0.9724 to 0.9859 at pH 5.2 and values between 0.9835 to 0.9879 at pH 7.5 indicating the first-order model released more drug compared to zero-order kinetics. These models demonstrated a good match because their calculated values were close to 1. The suitability assessment for all linear curves except Korsmeyer-Peppas model showed r2 values above 0.94. The main method by which this system transferred substances was identified as Fickian diffusion based on experimental test results. Fickian diffusion control mechanism manifests during Beta-Carotene release from SLNs which have been encapsulated with Beta-Carotene. Extensive analysis between these kinetic tests and the PSA test confirms first-order kinetics as a suitable fit for the release data of Beta-Carotene. Nanoparticle formulation breaks down uniformly leading to a slow release of its cargo according to the data recorded.

Stability studies of Beta-Carotene-encapsulated SLNs

The UV absorption spectra of Beta-Carotene-encapsulated Solid Lipid Nanoparticles (SLNs) appeared under diverse stabilizing conditions with a spectroscopic depiction. The researchers measured spectrum absorbance from 250 nm up to 350 nm. The maximum absorption wavelength (λ_{max}) varies based on the surrounding environment in the SLN system. The findings indicate λ_{max} equals 274 nm for 10 % NaCl solution with volume fraction weight ratio 10 percent. The highest λ_{max} value occurred when SLNs contained 0.5 % (w/v) BSA in ionic high-strength solutions and it may represent protein interaction effects. When SLNs existed in pH 5.2 acetate buffer and pH 7.5 phosphate buffer solution their λ_{max} value reached 282 nm maintaining the same peak. Gastric fluid containing enzymes and acids altered the λ_{max} value to 298 nm which indicates how the stomach conditions might influence

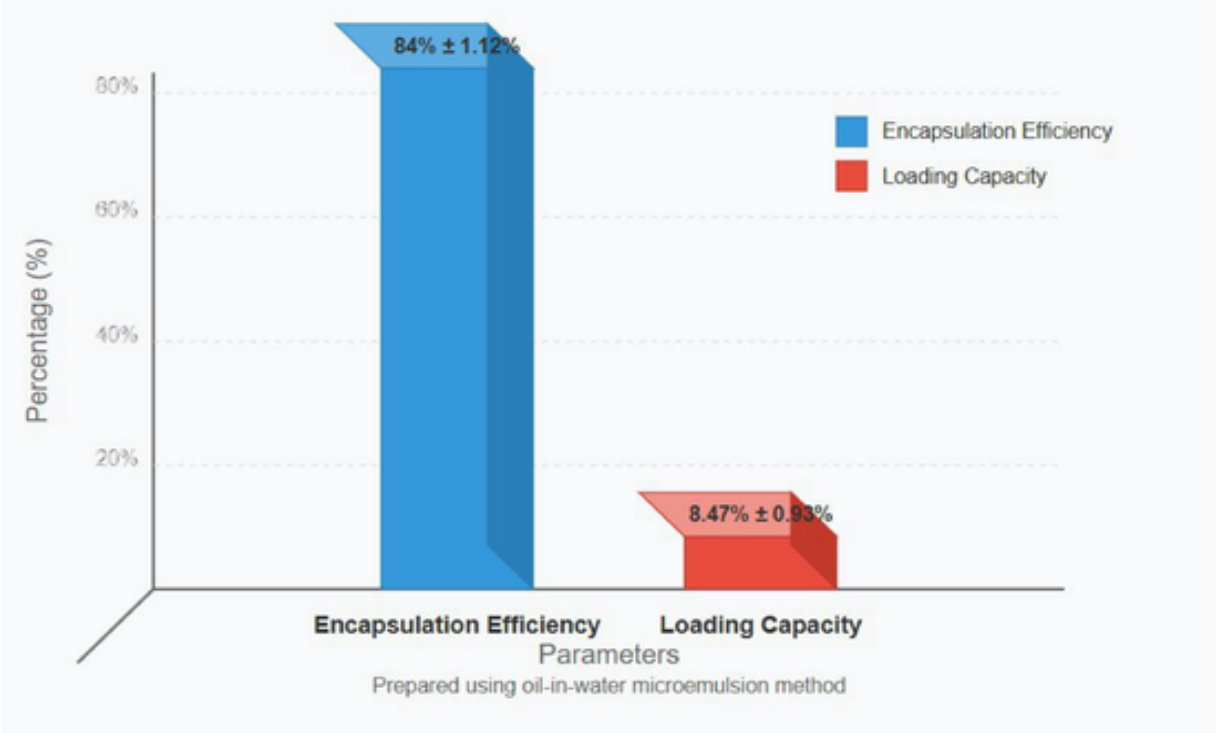

Fig. 6. Encapsulation efficiency and loading capacity of beta-carotene nanoparticles prepared using oil-in-water microemulsion method, showing 84 % ± 1.12 encapsulation efficiency and 8.47 % ± 0.93 loading capacity.

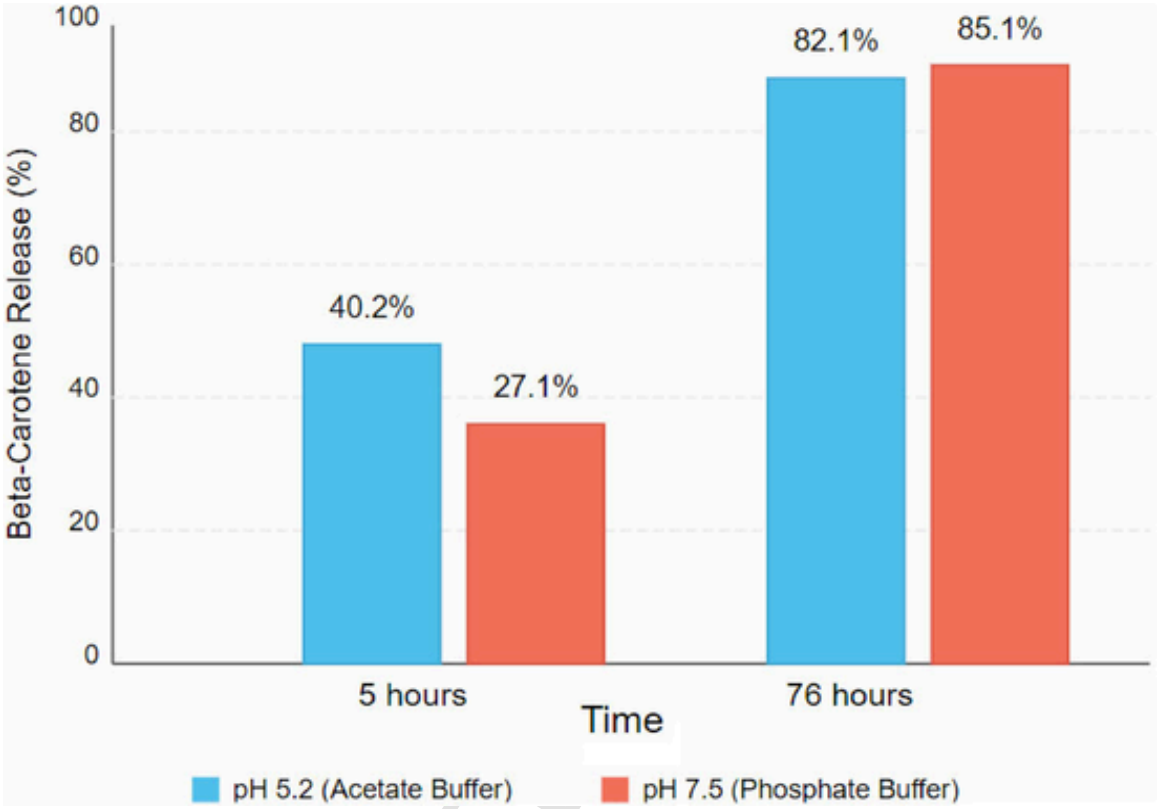

Fig. 7. Beta-carotene release profile in pH 5.2 acetate and pH 7.5 phosphate buffers at 5 and 76 h, showing enhanced release in alkaline conditions over prolonged duration.

the absorption behavior of SLNs. The absorption maxima of the different processing solutions display noticeable but tiny differences when observing the studied samples Fig. 9. This shows how well the SLN encapsulates respond to environmental atmospheric effects.

LC-MS analysis of Beta-Carotene-encapsulated SLNs

The LC-MS method indicates that SLNs containing Beta-Carotene extract exhibit active component which produce specific retention times alongside mass spectrometry peaks. The LC-MS system detects Beta-Carotene at a retention time of 3.1 min (m/z 536.87 ([M + H]) to indicate the extract contains Beta-Carotene. Results data confirm that this primary agent gets sufficiently incorporated and stays stable in the SLNs thus demonstrating appropriate loading under LC-MS conditions. The used method successfully encapsulates upgraded ingredients into SLNs while producing results free from background interferences to enable separate compound identification for each species. The described characteristics show that these SLNs can function as pharmaceutical drug delivery vehicles Fig. 10.

FE-SEM analysis of Beta-Carotene-encapsulated SLNs

In Fig. 11 researchers displayed the FE-SEM image of Beta-Carotene encapsulated SLNs to show their spherical shape along with the encapsulation achievement in the SLNs system. FE-SEM imaging displays spherical nanoparticles with plain surfaces along with uniform distribution patterns throughout which proves successful production and shell formation of SLNs. The identification of these nanoparticles demonstrates minimal agglomeration and smoothness since these properties enhance drug release reproducibility along with stability needed for drug delivery. SLN size homogeneity demonstrates that synthesis processes were controlled and delivered reproducible outcomes needed for achieving consistent drug therapy. The even surface distribution within FE-SEM images contains minimal surface defects that functions to decrease the risk of immediate drug release while controlling the time-dependent release of active compound (Beta-Carotene). Beta-Carotene demonstrates high levels of stability and bioavailability because the encapsulation process inside SLNs shows no evidence of drug degradation or leakage. The FE-SEM results demonstrate that the Beta-Carotene-encapsulated SLNs fulfill the necessary physical properties for drug carriers which boosts the delivery capabilities of Beta-Carotene.

FTIR analysis of Beta-Carotene-encapsulated SLNs

The molecular structure of β-carotene, as depicted in the image, is a tetraterpene compound naturally synthesized and widely recognized for its significant antioxidant properties in the diet. This compound consists of a polyene chain with eleven conjugated double bonds and two terminal β-ionone rings, giving it its characteristic structure. Due to the length of its conjugated polyene chain, β-carotene is endowed with its distinct deep orange color and remarkable ability to absorb visible light. This light absorption plays a critical role in various biological processes, including photosynthesis in plants and vision in humans. Structurally, β-carotene is composed entirely of nonpolar hydrocarbons and lacks oxygen-containing functional groups, which significantly influences its infrared (IR) spectral behavior, as shown in Fig. 12. In terms of IR spectroscopy, β-carotene exhibits a series of characteristic absorption bands that are indicative of its molecular structure. One of the primary features is the absorption band at 1694 cm^{-1}, which corresponds to the $C = C$ stretching vibrations of the conjugated double bonds in the polyene chain. Additional absorption bands are observed at 2856 cm^{-1} for the methyl and methylene C–H stretching vibrations, at 2922

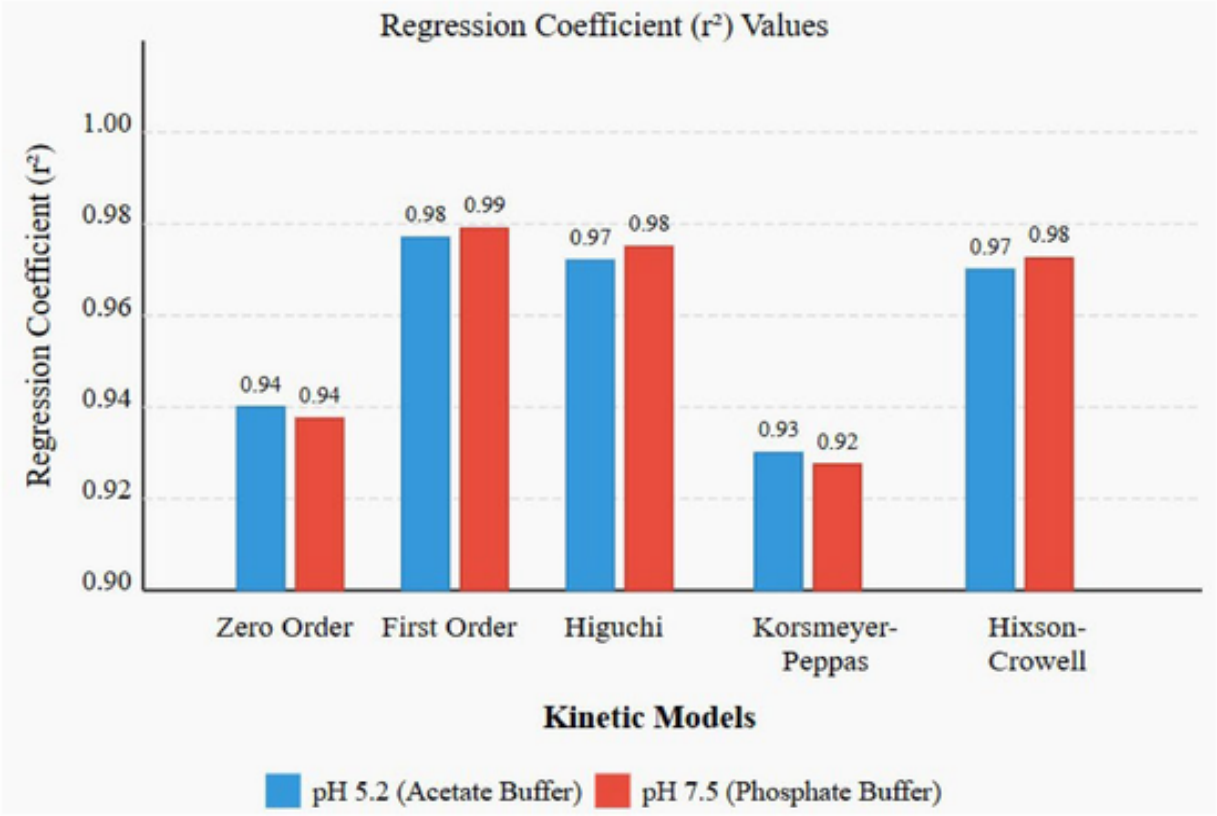

Fig. 8. Comparative regression coefficient (r^2) values of drug release kinetic models in pH 5.2 acetate and pH 7.5 phosphate buffers, indicating best fit with First Order and Higuchi models.

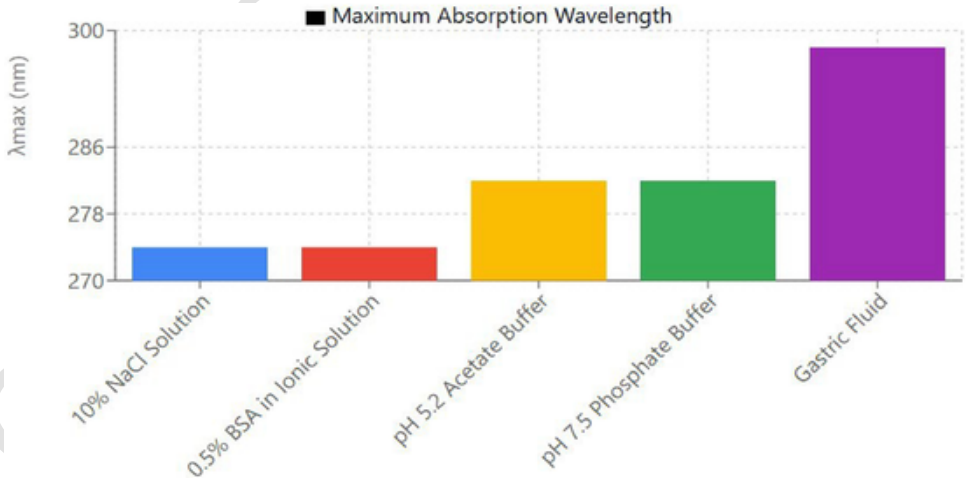

Fig. 9. Maximum absorption wavelength (λ_{max}) of the sample in various media, showing increased λ_{max} in gastric fluid, indicating environmental influence on compound stability and spectral behaviour under different physiological conditions.

cm^{-1} for aromatic C–H stretching, and at 1456 cm^{-1} for methyl C–H bending vibrations. Furthermore, out-of-plane $=C—H$ bends characteristic of trans-disubstituted alkenes are detected in the 978 cm^{-1} region. Notably, the absence of broad O—H or sharp $C = O$ peaks further reinforce the hydrocarbon nature of β-carotene. The distinct IR absorption patterns of β-carotene provide valuable information for identification, purity confirmation, and quality control in both analytical and formulation applications. By analyzing these absorption bands, researchers can effectively verify the purity of β-carotene and ensure its consistency in pharmaceutical and nutraceutical formulations. The unique spectral characteristics make IR spectroscopy a reliable technique for assessing the chemical integrity and structural identity of β-carotene in various product applications.

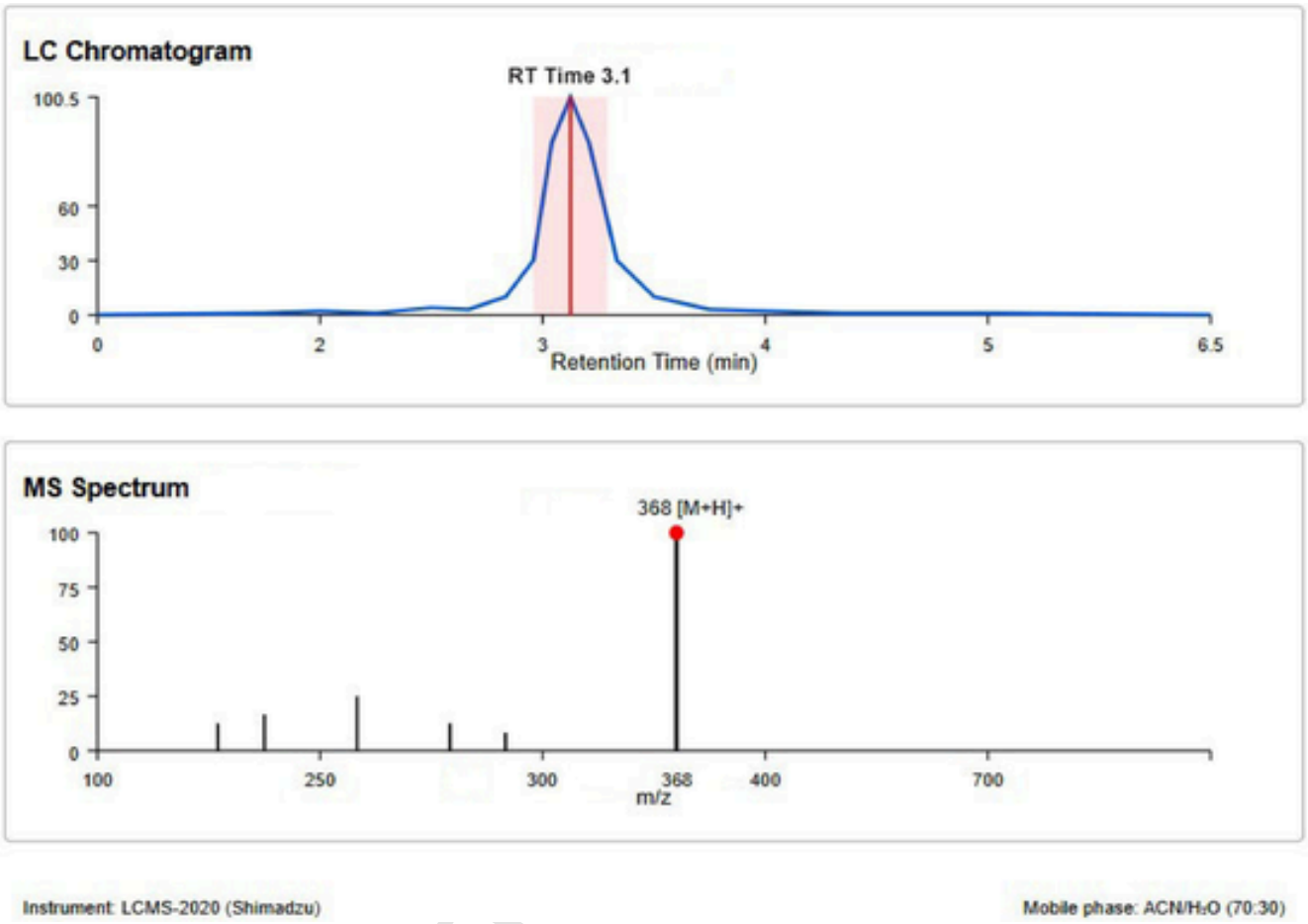

Fig. 10. LC-MS analysis showing LC chromatogram with retention time at 3.1 min and MS spectrum indicating molecular ion peak at *m/z* 368 [*M* + H]+ using ACN:H_2O (70:30) mobile phase.

MTT assay

The effectiveness of β-carotene to kill the tested cells was evaluated with respect to the MTT assay at various concentrations (6.25, 12.5, 50 μg/mL, 25, and 100 μg/mL). There was a significant reduction in cell viability that was as a result of increased β –carotene concentrations as shown in the results. Mean percentage viability at the concentration of 6.25 μg/mL was 73.13 %, dropping to 63.33 % with an amount increase to 12.5 μg/mL. When the cells were treated at 25 μg/mL, percentage of viable cells considerably reduced to 44.6 %. At the higher doses used at 50 μg/mL and 100 μg/mL, the cell survival continued to decline at 35.53 % and 26.46 % respectively. The IC_{50} value established was 22.82 μg/mL, which indicated an intermediate cytotoxicity in the action of β-carotene against the studied cells. This was further evidence of the quantitative result found through observation of the treated cells under the microscope. Control cells had a healthy appearance and densely packed cell densities and normal morphology. As the dose of β-carotene was increased, a reduction of the density of cells that accompanied the morphological changes (shrinkage, rounding, disassociation) was observed particularly at the concentrations of 50 and 100 μg/mL. Such observations implicate cytotoxic induction with manifestation in the form of either apoptosis or necrosis. The statistical assessment over every concentration resulted in reproducible observations, with only minor differences in the data especially at the 6.25 μg/mL with a variance of 0.1688. Collectively, the data show that β-carotene exhibits concentration-dependent cytotoxic activity, which validates its conformance to the morphological changes that have been exhibited through microscopy and confirms the possibility that β-carotene is capable of inhibiting the proliferation of cells Fig. 13.

Conclusion

Finally, it can be concluded that the present study shows the promising perspectives for using beta-carotene encapsulated in SLNs for targeted therapy of breast cancer. According to the results of in silico and in vitro studies, beta-carotene has the ability to interact with the crucial oncogenic proteins, induce apoptosis and prevent cancer cells from proliferating. The molecular docking and dynamics simulation furnish an explanation at high depth regarding the protein-ligand interactions, which validate the stability of the beta–carotene complex with the crucial residues that participate in binding. Indeed, the strong binding affinity and relatively stable interactions with target proteins are added advantages to its potential to become a good therapeutic agent. The results of the ADMET analysis as pharmacokinetic properties of beta-carotene demonstrate the favorable characteristics of the compound for the purposes of drug delivery, namely, being well absorbed in the gastrointestinal tract, highly bioavailable, despite the lipophilicity and the size of cellular material. The encapsulation efficiency of 84 ± 1.12 % and drug loading capacity of 8.47 ± 0.93 % suggest stable and effective delivery system (SLNs) for improving the bioavailability of beta-carotene. In vitro release studies reveals that the controlled release of beta carotene from the SLNs occurs with a maximum release of 85.12 % at pH 7.5 during 76 h, indicated the potential of sustained drug release. The release kinetics obeys first order model which indicated a diffusion

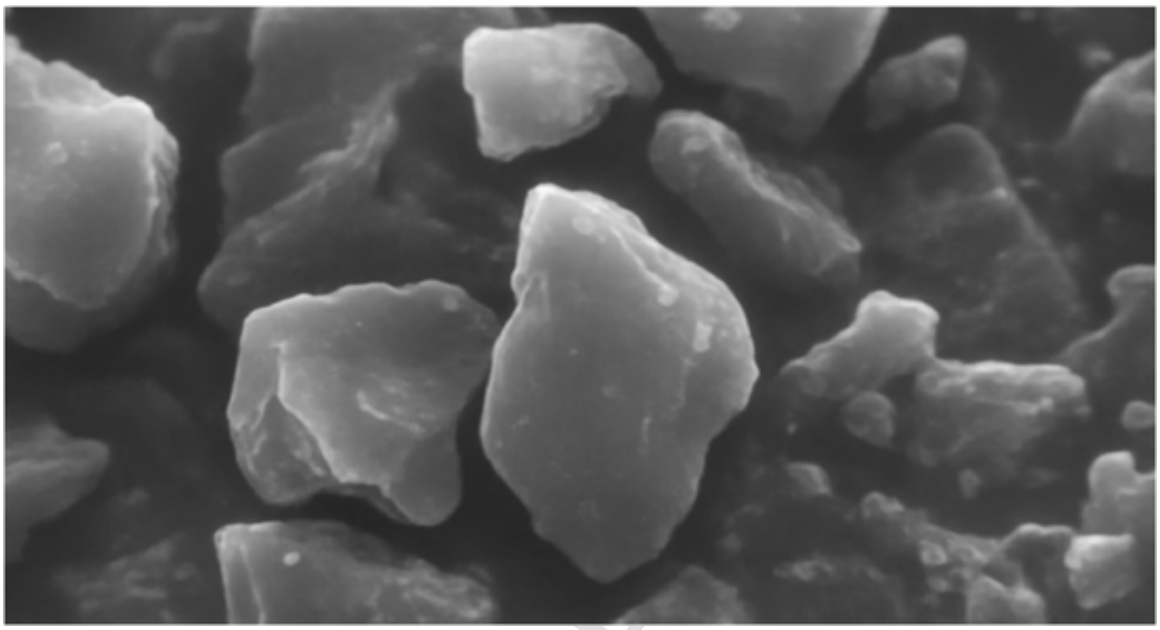

Fig. 11. Scanning electron microscope (SEM) image displaying a highly magnified view of a surface with rough, wrinkled texture, coated with small particulate matter. The image is captured at 40,000x magnification.

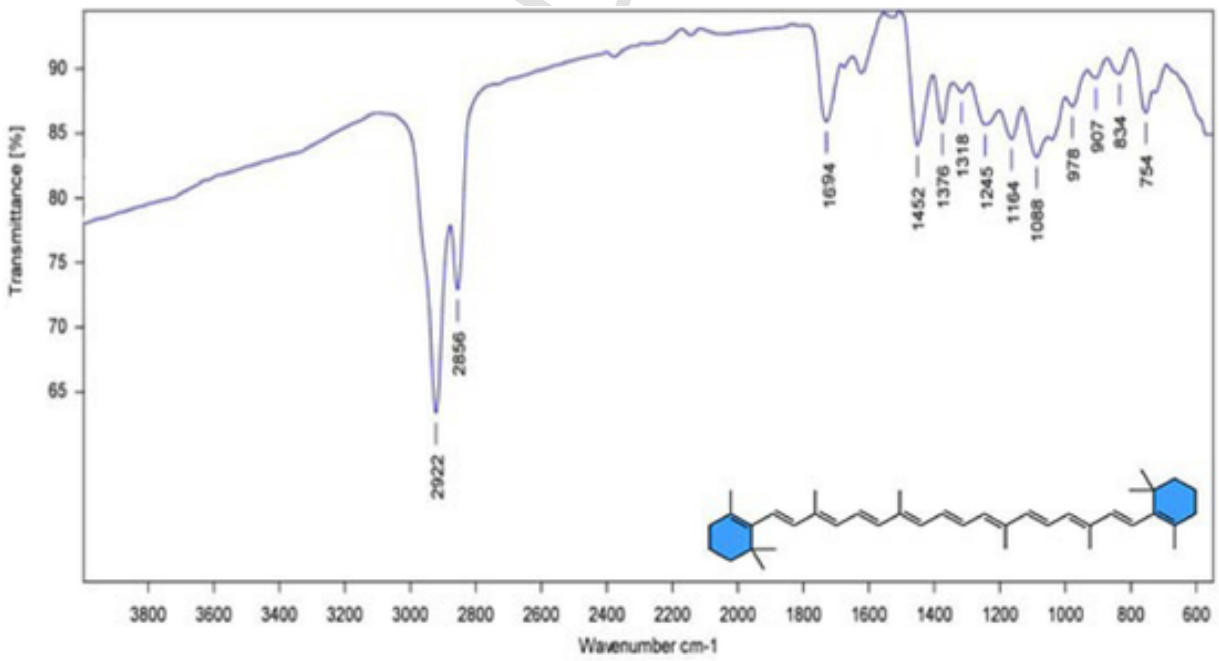

Fig. 12. Scanning electron microscope (SEM) image displaying a highly magnified view of a surface with rough, wrinkled texture, coated with small particulate matter. The image is captured at 40,000x magnification.

control mechanism. Cytotoxicity of beta-carotene was determined by MTT assay and an IC_{50} value of 22.82 ug/mL was obtained, significantly suggesting moderate cytotoxicity against MCF-7 breast cancer cells. All in all, the results of this study indicate that the use of beta-carotene-loaded SLNs may be a perspective approach to breast cancer therapy. The positive encapsulation efficiency, controlled release, as well as moderate cytotoxicity confirm its possible use as support of the conventional therapies. Additional clinical studies would be required to confirm its therapeutic efficacy and development of the formulation for clinical uses.

CRediT authorship contribution statement

Kandanagolla Sumalatha: Writing – review & editing, Writing – original draft, Methodology, Conceptualization. **Panneerselvam Theivendren:** Writing – review & editing, Writing – original draft, Validation, Supervision, Software. **Gandhimathi Rathinasamy:**

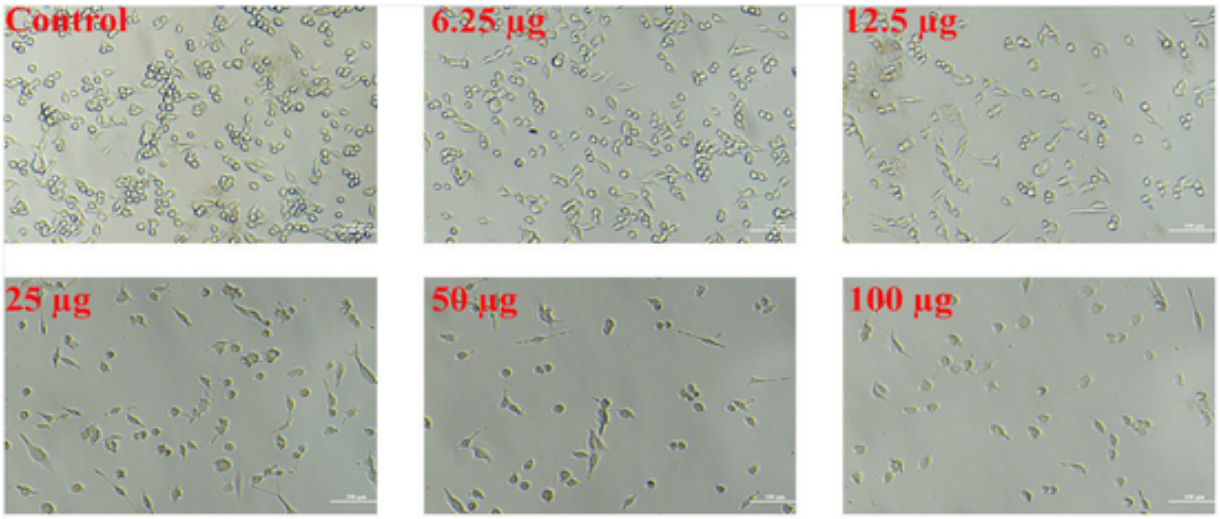

Fig. 13. The cell morphology under a microscope following treatment with various concentrations (6.25 µg, 12.5 µg, 25 µg, 50 µg, 100 µg) compared to the control group. Scale bar: 200 µm.

Writing – review & editing, Writing – original draft, Visualization, Validation, Supervision, Conceptualization.

Declaration of competing interest

The authors declare that they have no known competing financial interests or personal relationships that could have appeared to influence the work reported in this paper.

Acknowledgement

We sincerely acknowledge the Department of Pharmaceutical Chemistry & Analysis, School of Pharmaceutical Sciences, Vels Institute of Science, Technology & Advanced Studies, Pallavaram, Chennai, Tamil Nadu, for their invaluable support and guidance.

Data availability

No data was used for the research described in the article.

References

[1] Goldberg J, Pastorello RG, Vallius T, Davis J, Cui YX, Agudo J, Waks AG, Keenan T, McAllister SS, Tolaney SM. The immunology of hormone receptor positive breast cancer. Front Immunol 2021;12:674192.
[2] Smolarz B, Nowak AZ, Romanowicz H. Breast cancer—Epidemiology, classification, pathogenesis and treatment (review of literature). Cancers 2022;14 (10):2569.
[3] Mao J, Hu J, Zhang Y, Shen J, Dong F, Zhang X, Ming J, Huang T, Run X. Single hormone receptor-positive metaplastic breast cancer: similar outcome as triple-negative subtype. Front Endocrinol 2021;12:628939.
[4] Cao L, Niu Y. Triple negative breast cancer: special histological types and emerging therapeutic methods. Cancer Biol Med 2020;17(2):293–306.
[5] Yin L, Duan J-J, Bian X-W, Yu S-C. Triple-negative breast cancer molecular subtyping and treatment progress. Breast Cancer Res 2020;22:1–13.
[6] Luo L, Keyomarsi K. PARP inhibitors as single agents and in combination therapy: the most promising treatment strategies in clinical trials for BRCA-mutant ovarian and triple-negative breast cancers. Expert Opin Investig Drugs 2022;31(6): 607–31.
[7] Zhang J, Zhang J, Li H, Chen L, Yao D. Dual-target inhibitors of PARP1 in cancer therapy: a drug discovery perspective. Drug Discov Today 2023;28(7):103607.
[8] Dilmac S, Ozpolat B. Mechanisms of PARP-inhibitor-resistance in BRCA-mutated breast cancer and new therapeutic approaches. Cancers 2023;15(14):3642.
[9] Dhakad GG, Patil GD, Nikum AC, Shirsat SP. Review on radiation therapy on cancer. Res J Pharmacol Pharmacodyn 2022;14(1):4–12.
[10] Cortesi L, Rugo HS, Jackisch C. An overview of PARP inhibitors for the treatment of breast cancer. Target Oncol 2021;16(3):255–82.
[11] Barchiesi G, Roberto M, Verrico M, Vici P, Tomao S, Tomao F. Emerging role of PARP inhibitors in metastatic triple negative breast cancer. Current scenario and future perspectives. Front Oncol 2021;11:769280.
[12] Barakat AZ, Hamed AR, Bassuiny RI, Abdel-Aty AM, Mohamed SA. Date palm and saw palmetto seeds functional properties: antioxidant, anti-inflammatory and antimicrobial activities. J Food Measand Char 2020;14(2):1064–72.
[13] Mohamed SA, El-Shishtawy RM, OAM Al-Bar, AR Al-Najada. Chemical modification of curcumin: solubility and antioxidant capacity. Int J Food Pro 2017; 20:718–24.
[14] Ferlay J, Colombet M, Soerjomataram I, Parkin DM, Piñeros M, Znaor A, Bray F. Cancer statistics for the year 2020: an overview. Int J Cancer 2021;149(4):778–89.
[15] Kunjiappan S, Panneerselvam T, Somasundaram B, Arunachalam S, Sankaranarayanan M, Parasuraman P. Preparation of liposomes encapsulated Epirubicin-gold nanoparticles for tumor specific delivery and release. Biomed Phys Eng Express 2018;4(4):045027.
[16] Shin J, Song M-H, Oh J-W, Keum Y-S, Saini RK. Pro-oxidant actions of carotenoids in triggering apoptosis of cancer cells: a review of emerging evidence. Antioxidants 2020;9(6):532.
[17] Zhao G, Zhang X, Wang H, Chen Z. Beta carotene protects H9c2 cardiomyocytes from advanced glycation end product-induced endoplasmic reticulum stress, apoptosis, and autophagy via the PI3K/Akt/mTOR signaling pathway. Ann Transl Med 2020;8(10):647.
[18] Bizuayehu HM, Dadi AF, Hassen TA, Ketema DB, Ahmed KY, Kassa ZY, Amsalu E, Kibret GD, Alemu AA, Alebel A. Global burden of 34 cancers among women in 2020 and projections to 2040: population-based data from 185 countries/territories. Int J Cancer 2024;154(8):1377–93.
[19] Boukhatem MN, Setzer WN. Aromatic herbs, medicinal plant-derived essential oils, and phytochemical extracts as potential therapies for coronaviruses: future perspectives. Plants 2020;9(6):800.
[20] Sun W, Shahrajabian MH. Therapeutic potential of phenolic compounds in medicinal plants—natural health products for human health. Molecules 2023;28 (4):1845.
[21] Abeysinghe D, Alwis D, Kumara K, Chandrika U. Nutritive importance and therapeutics uses of three different varieties (Murraya koenigii, Micromelum minutum, and Clausena indica) of curry leaves: an updated review. Evid-Based Complement Altern Med 2021;2021(1):5523252.
[22] Chaudhary A. A review on the culinary uses and therapeutic properties of Murraya koenigii. J Adv Pharmacol 2020;1(1):1–8.
[23] Kalimuthu AK, Parasuraman P, Sivakumar P, Murugesan S, Arunachalam S, Pandian SRK, Ravishankar V, Ammunje DN, Sampath M, Panneerselvam T. In silico, in vitro screening of antioxidant and anticancer potentials of bioactive secondary metabolites from an endophytic fungus (Curvularia sp.) from Phyllanthus niruri L. Env Sci Pollut Res 2022;29(32):48908–25.
[24] Panneerselvam T, Kunjiappan S, Govindaraj S, Gopal M, Natarajan K, Hegde YM, Shanmugam N, Srinivas G, Ravi K, Natarajan V. Graph theoretical analysis, in silico modeling and molecular dynamic studies of (5-((2-chloropyridin-4-yl) oxy)-3-phenyl-1H-pyrazol-1-yl)-2- (4-substituted phenyl)-N, N-dimethylethen-1-amine derivatives for the treatment of breast cancer. Anti-Cancer Agents Med Chem 2022.
[25] Palanichamy C, Pavadai P, Panneerselvam T, Arunachalam S, Babkiewicz E, Ram Kumar Pandian S, Shanmugampillai Jeyarajaguru K, Nayak Ammunje D, Kannan S, Chandrasekaran J. Aphrodisiac performance of bioactive compounds from *Mimosa pudica* Linn.: in silico molecular docking and dynamics simulation approach. Molecules 2022;27(12):3799.
[26] Mandhadi JR, Panneerselvam T, Parasuraman P. DESIGN, In silico modeling, toxicity study and synthesis of novel substituted semicarbazide derivatives of pyrimidine: an antitubercular agent. Curr Bioact Compd 2020;16(3):294–301.

[27] Rajeshkumar RR, Kumar BK, Parasuraman P, Panneerselvam T, Sundar K, Ammunje DN, Pandian SRK, Murugesan S, Kabilan SJ, Kunjiappan S. Graph theoretical network analysis, in silico exploration, and validation of bioactive compounds from *Cynodon dactylon* as potential neuroprotective agents against α-synuclein. BioImpacts 2022;12(6):487.
[28] Saravanan G, Panneerselvam T, Kunjiappan S, Parasuraman P, Alagarsamy V, Udayakumar P, Soundararajan M, Joshi SD, Ramalingam S, Ammunje DN. Graph theoretical analysis, in silico modeling, prediction of toxicity, metabolism and synthesis of novel 2-(methyl/phenyl)-3- (4- (5-substituted-1, 3, 4-oxadiazol-2-yl) phenyl) quinazolin-4 (3H)-ones as NMDA receptor inhibitor. Drug Dev Res 2019;80 (3):368–85.
[29] Almeida SD, Ramesh SH, Radhakrishna GK, Sireesha G, Ramesh S, Kumar BS, Hosur Dinesh BG, Ganjipete S, Nagaraj S, Theivendren P. Development and evaluation of S-carboxymethyl-L-cystine-loaded solid lipid nanoparticles for Parkinson's disease in murine and zebrafish models. Sci Rep 2025;15(1):10885.
[30] Kunjiappan S, Sankaranarayanan M, Kumar BK, Pavadai P, Babkiewicz E, Maszczyk P, Glodkowska-Mrowka E, Arunachalam S, Pandian SRK, Ravishankar V. Capsaicin-loaded solid lipid nanoparticles: design, biodistribution, in silico modeling and in vitro cytotoxicity evaluation. Nanotechnology 2020;32(9): 095101.
[31] Pandian SRK, Pavadai P, Vellaisamy S, Ravishankar V, Palanisamy P, Sundar LM, Chandramohan V, Sankaranarayanan M, Panneerselvam T, Kunjiappan S. Formulation and evaluation of rutin-loaded solid lipid nanoparticles for the treatment of brain tumor. Naunyn-Schmiedeb Arch Pharmacol 2021;394:735–49.